Ice nucleation from drop-freezing experiments: Impact of droplet volume dispersion and cooling rates

Ravi Kumar Reddy Addula*[1], Ingrid de Almeida Ribeiro*[2], Valeria Molinero[2], and Baron Peters[1,3]

[1]Chemical and Biomolecular Engineering, University of Illinois at Urbana-Champaign, Urbana, IL 61801, USA.
[2]Department of Chemistry, The University of Utah, Salt Lake City, UT 84112, USA.
[3]Department of Chemistry, University of Illinois at Urbana-Champaign, Urbana, IL 61801, USA.

Correspondence: Baron Peters (baronp@illinois.edu)

Abstract. Because homogeneous ice nucleation is important for atmospheric science, special assays have been developed to monitor ultra-pure nanoscale water droplets for nucleation as the temperature is gradually lowered to deeply supercooled conditions. To analyze the experimental data and predict droplet freezing, we develop model that accounts for the cooling rate and the distribution of droplet sizes. We use the model to analyze two sets of experimental homogeneous nucleation data with carefully controlled cooling rates and droplet sizes. Rate expressions based on classical nucleation theory describes both experiments well and with rate parameters in approximate agreement with theoretical predictions based on the thermodynamics of water. We further demonstrate that a failure to account for dispersion in droplet volumes reduces the apparent barriers for ice nucleation. We provide an open source code to estimate nucleation parameters from drop-freezing assays, and another code to account for dispersion of droplet volumes and predict the outcome of drop-freezing experiments. We also present a sensitivity analysis to find the effect of temperature uncertainty on the measured nucleation spectrum. Our framework may be directly useful in accounting for droplet polydispersity and cooling rates for ice nucleation in clouds. Although our analysis pertains to homogeneous nucleation, we note that similar strategies may be applied to heterogeneous ice nucleation on minerals and organic particles with variable surface areas and nucleation sites.

1 Introduction

The thermodynamics and kinetics of ice formation from water are important for atmospheric science (Koop et al. (2000); Möhler et al. (2007); DeMott et al. (2010); Knopf and Alpert (2023)), preservation of biologically active substances (John Morris et al. (2012); Zachariassen and Kristiansen (2000)), and storage of food products (Goff (1997); Li and Sun (2002)). Nucleation, the first step in ice formation, heralds the onset of important subsequent changes: rapid growth of ice domains (Shultz (2018); Barrett et al. (2019); Sibley et al. (2021)), the release of latent heat (Riechers et al. (2013); Dobbie and Jonas (2001)), and freeze concentration of impurities (Deck et al. (2022); Deville (2017); Stoll et al. (2021)). A quantitative understanding

*These authors contributed equally to this work

of these processes requires models that accurately predict ice nucleation kinetics. In most applications, the primary source of nuclei is heterogeneous nucleation on various surfaces and impurities at mild supercooling (Alpert and Knopf (2016); Zhang and Maeda (2022); Stan et al. (2009); Kubota (2019)). However, homogeneous nucleation of ice occurs at deep supercooling for highly pure water droplets in the atmosphere (Koop et al. (2000); Knopf and Alpert (2023)) and in certain laboratory experiments (Murray et al. (2010); Atkinson et al. (2016); Shardt et al. (2022); Riechers et al. (2013); Laksmono et al. (2015)).

Special assays have been developed to study ice nucleation kinetics by monitoring hundreds of small supercooled water droplets (Laval et al. (2009); Shardt et al. (2022); Ando et al. (2018); Tarn et al. (2020)). These experiments provide an independent realization of the nucleation time and/or temperature for each droplet (Tarn et al. (2020); Shardt et al. (2022)). Typically, the kinetics are studied via induction times in isothermal conditions (constant supercooling) (Alpert and Knopf (2016); Herbert et al. (2014); Knopf et al. (2020)) or via the spectrum of nucleation temperatures at constant cooling rate (Zhang and Maeda (2022); Ando et al. (2018); Shardt et al. (2022); Murray et al. (2010)). These two types of experiments have important similarities and differences.

For droplets subjected to a constant supercooling, the induction time is exponentially distributed. Several analyses have modeled the exponential decay to understand how nucleation rates depend on supercooling (Alpert and Knopf (2016); Herbert et al. (2014); Knopf et al. (2020)). In experiments where the supercooling is gradually increased, the distribution of nucleation times is more complicated (Murray et al. (2010); Riechers et al. (2013)). Typically, no nucleation events occur until the temperature drops below some critical temperature, and then the nucleation times/temperatures all occur within a focused range (Murray et al. (2010); Riechers et al. (2013); Shardt et al. (2022)). To motivate new elements of our model, we briefly discuss the capabilities and gaps in existing models for analyzing the experiments with steadily cooled droplets.

Analyses of drop-freezing experiments can be grouped according to two distinguishing criteria. The first distinction pertains to the models used for interpreting the nucleation rate. Kubota used empirical nucleation rate models (Kubota (2019)), while others have used theoretically motivated rate expressions (often based on classical nucleation theory) (Ickes et al. (2017); Murray et al. (2010); Riechers et al. (2013)). Empirical rate models can provide excellent fits to the nucleation rate data, and successful empiricisms sometimes inspire new theoretical models. However, the fitted rate expressions for nucleation rate from an empirical model lack the interpretability and generalizability afforded by a successful fit to theoretical rate models.

A second distinction pertains to the analysis and interpretation of the droplet nucleation data itself. Some studies focus on the fraction of droplets that nucleate in a specific supercooling range, i.e. the nucleation spectrum (Murray et al. (2010); Shardt et al. (2022); Ando et al. (2018)). The nucleation spectrum has sometimes been interpreted as an intrinsic property of supercooled water and/or the nucleants present in the system (Zhang and Maeda (2022); Alpert and Knopf (2016); Knopf and Alpert (2023)). However, it also depends on variables beyond chemical or interfacial properties, e.g. the cooling rates and droplet sizes. An alternative explanation for the nucleation spectrum begins with the survival probability formalism. In survival probability analyses, the probability that a droplet remains liquid steadily declines with time in proportion to the changing rate of ice nucleation. The survival probability formalism is easily used in combination with theoretical models for the nucleation rate, but the combination remains rare in the ice nucleation literature. Indeed, prior combinations of survival probability and

nucleation theory in the ice literature focus on heterogeneous nucleation (Wright and Petters (2013); Marcolli et al. (2007); Alpert and Knopf (2016)).

In this work, we combine survival probability analysis with classical nucleation theory to quantitatively predict the effects of different droplet volumes (Atkinson et al. (2016)) and cooling rates (Shardt et al. (2022)). The experiments that motivated our study observed homogeneous nucleation in narrowly sized selected droplets, cooled at a steady rate deep into the metastable zone. We are inspired by the experiments to achieve the precise control of droplet sizes, but the atmospheric clouds will naturally have a distribution of droplet sizes (Painemal and Zuidema (2011)). We demonstrate a method to extract theoretically derived nucleation rate parameters from the experimental survival probability data of monodispersed droplets and droplets with the distribution of sizes. The analysis shows that experimental measurements are consistent with predictions of classical nucleation theory across a range of supercooling, droplet sizes, and cooling rates.

2 Analytical model to analyze the nucleation of monodispersed droplets

The probability that a single droplet of volume V is not frozen in a given time t can be modelled using the master equation (Cox and Oakes (1984)).

$$\frac{dP(t|V)}{dt} = -P(t|V) \times JV. \tag{1}$$

Here $P(t|V)$ is the probability, J is the nucleation rate on a per volume per time basis, and V is the droplet volume. The temperature is constant and the rate of nucleation in each liquid droplet also remains constant in induction time measurements. On integrating Eq. (1) survival probability becomes $P(t|V) = \exp[-JVt]$. This result has been used to analyze nucleation data in several crystallization studies, e.g. by plotting $\ln p(t|V)$ vs t to estimate J and its supersaturation dependence (Alpert and Knopf (2016); Knopf and Alpert (2023); Stöckel et al. (2005); Kubota (2019); Sear (2014)). In contrast, in experiments where the supercooling increases with time, the nucleation rate in each liquid droplet also increases with time. The survival probability can be obtained by integrating Eq. (1), we get

$$P(t|V) = \exp\left[-\int_0^t J(t)V\,dt\right], \tag{2}$$

where P as a function of time, but the data are usually reported as a function of temperature or supercooling (Murray et al. (2010); Shardt et al. (2022)). Since the experiments are conducted at a specific cooling rate R (Murray et al. (2010); Shardt et al. (2022)), we replace the time variable with temperature using the following relation

$$T = T_m - R \times t. \tag{3}$$

After variable transformation the survival probability becomes

$$P(T|V) = \exp\left[-\frac{V}{R}\int_{T_m}^{T} J(T')dT'\right] \tag{4}$$

Eq. (4) separates protocol-specific factors (droplet size and cooling rate) from intrinsic properties of the nucleation kinetics and their dependence on temperature.

Now, we need theoretical models or experimental data for nucleation rate to predict the survival probability. Classical nucleation theory gives the rate for homogeneous nucleation as (Volmer and Weber (1926); Becker and Döring (1935))

$$J = A\exp\left[-\frac{16\pi\gamma^3 v_0^2}{3(\lambda_f^2/T_m^2)k_B T}\left(\frac{1}{T_m - T}\right)^2\right], \tag{5}$$

where A is the kinetic prefactor, γ is the interfacial free energy between the ice and water, λ_f is the latent heat of ice, k_B is the Boltzmann constant, T_m is the melting point of ice, v_0 is the molar volume of ice and T is the absolute temperature.

To account for the temperature dependence of nucleation and the time-dependent temperature, one must carefully separate the temperature-dependent and temperature-independent parts of J. Using $\delta_T = (T_m - T)/T_m$ as the dimensionless temperature, we rewrite the expression for J as

$$J = A\exp\left[\frac{-B}{(1-\delta_T)\delta_T^2}\right], \tag{6}$$

where $B = (16\pi\gamma^3 v_0^2)/(3\lambda_f^2 k_B T_m)$ depends on properties of ice and water that are nearly independent of temperature for the narrow temperature range where homogeneous nucleation is observed in experiments (Kashchiev (2000); Sear (2007); Koop et al. (2000)). The parameters A and B are assumed to be temperature-independent in the present model. The term $(B/[(1-\delta_T)\delta_T^2])$ in the exponential denotes the free energy barrier for nucleation, and Eq. (6) shows how it depends on temperature. Using Eq. (6) in Eq. (4), the survival probability becomes

$$P(\delta_T|V) = \exp\left[-\left(\frac{AVT_m}{R}\right)\int_0^{\delta_T}\exp\left(\frac{-B}{(1-\delta_T')\delta_T'^2}\right)d\delta_T'\right]. \tag{7}$$

To our knowledge, Eq. (7) has not been used in previous studies of ice nucleation. It isolates parameters B, a property of nucleation kinetics, from the dimensionless group (AVT_m/R). The latter depends on intrinsic properties of ice and water (A and T_m) but also on environmental choices like V and R. Eq. (7) is valid for water droplets of volume V. In most experiments, there is a distribution of volumes which leads to a distribution of droplet nucleation rates. We consider the distribution of volume case in section 5, but first, we demonstrate that the model can predict the effect of droplet volume for narrowly size-selected droplets.

Across the range of nucleation temperatures observed in experimentsAtkinson et al. (2016); Shardt et al. (2022) for homogeneous ice nucleation (234 K - 238 K), the factor $(1-\delta_T)$ in the rate expression is always near 0.9. Hence, the nucleation rate expression is approximately $J = A\exp(B'/\delta_T^2)$. Where B' is approximately $B' = B/(1-\delta_T) \approx 1.1B$. With this approximation, we have an analytical solution for the survival probability as follows

$$\ln[P(\delta_T|V)] \approx \left[\frac{A'VT_m}{R}\right]\delta_T \times \left(\frac{\sqrt{\pi B'}}{\delta_T}\text{erfc}\left[\frac{\sqrt{B'}}{\delta_T}\right] - \exp\left[\frac{-B'}{\delta_T^2}\right]\right). \tag{8}$$

To illustrate the use of Eq. (7) and Eq. (8), we analyze one of the survival probability data sets (droplet size corresponding to 3.8-6.2 μm) obtained from Atkinson et al. (2016). Optimized fits of the analytical solution (Eq. (8), with $A' = 1.76 \times$

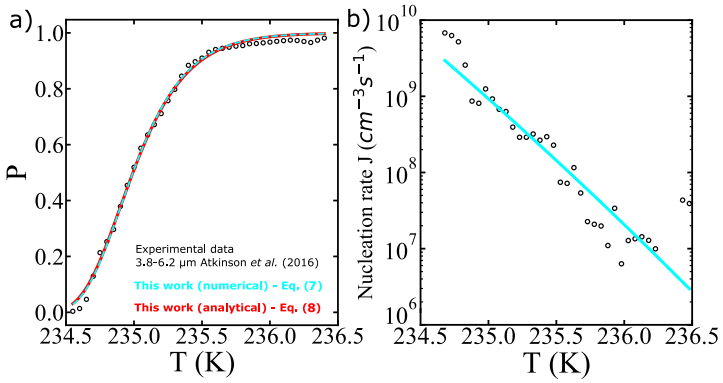

Figure 1. a) Illustration of survival probability fits with analytical (red continuous line) and numerical (cyan dashed line) solutions for the integral in Eq. (7). The experimental data represented by the empty black circles used as a reference is from Atkinson et al. (2016). b) Comparison of estimated nucleation rates from experiments using survival probability data as described in Atkinson et al. (2016) (black circles), and the nucleation rate computed using Eq. (7) (cyan line).

$10^{39} cm^{-3} s^{-1}, B' = 1.3578$) and the numerical integration (Eq. (7), with $A = 8.68 \times 10^{41} cm^{-3} s^{-1}, B = 1.2722$) are shown in Fig. 1. Even though the fits show excellent agreement in both analytical and numerical approaches, we note that a 10 % error in the exponent (from approximating $1 - \delta_T \approx 1.0$ leads to a nearly 1000-fold error in A' and a 10 % error in B' relative to A and B). We conclude that precise A and B values require careful treatment of even weak temperature dependencies within J. Although the prefactor and barriers are different, the predicted nucleation rates are not. For example, at 234.9 K both approaches give an estimate of nucleation rate to be $1.44 \times 10^9 cm^{-3} s^{-1}$.

The noisy estimates of J in Fig. 1b have been obtained by a finite difference of the cumulative survival probability data. For the finite difference procedure, large numbers of droplets are needed to obtain an estimate of J from the incremental nucleation events in each ΔT interval. As seen in Fig. 1b, there is considerable noise in the J estimates even in an experiment with hundreds of droplets. Our data analysis approach directly fits a model to the cumulative fraction of frozen droplets. It should therefore remain accurate for data sets with smaller numbers of droplets.

3 A computer code for analysis of drop-freezing experiments

We implemented the numerical integration in Eq. (7) and analytical model of Eq. (8) in an python code to estimate A, B and J from experimental drop-freezing data. The code outputs the parameters A and B from Eq. (7). These are used to compute the nucleation barriers ΔG, the temperature that corresponds to 50% of frozen droplets T_{50}, and the homogeneous nucleation rate evaluated at T_{50} using $J_{hom}^{model}(\delta_T) = A\, e^{-B/[(1-\delta_T)\delta_T^2]}$. The AINTBAD (Analysis of Ice nucleation Temperature for B and A Determination) code is illustrated in Fig. 2. The code is available in (https://github.com/Molinero-Group/volume-dispersion), last access: 18 Mar 2024).

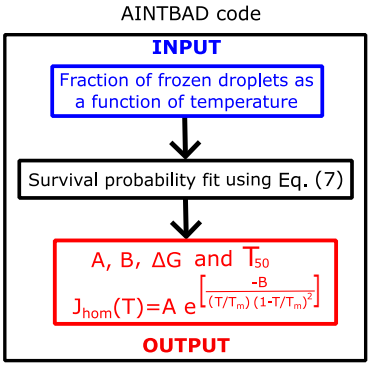

Figure 2. Flowchart of the AINTBAD (Analysis of Ice nucleation Temperature for B and A Determination) code.

We use the minimize function from the *scipy.optimize* module in Python to optimize the difference between the target survival probability and the predicted one by adjusting the parameters A and B. The chosen optimization method is the Nelder-Mead algorithm, suitable for functions without explicit derivatives. Optional settings include a convergence tolerance of 10^{-4} and a maximum iteration limit of 1000.

4 Analysis of nucleation spectrum in mono dispersed droplets

Atkinson et al. (2016) monitored the freezing temperatures of narrowly size-selected droplets cooled to temperatures near 235 K at a steady rate of 1.0 $K\text{min}^{-1}$. The range of droplet sizes in each experiment and the fraction of droplets that remain at each temperature can be seen as data points in Fig. 3a. We have analyzed the data from Atkinson et al., in two ways. First, we separately fitted the data for each size range to Eq. (7). Because the range of sizes each size-selected group is narrow, we have assumed that all droplets in each size range are spheres with the mean diameter for that range. These fits (not shown) result in independent estimates of the optimized nucleation prefactor A and the barrier parameter B from each of the six experiments. Table 1 shows the range of droplet sizes in each experiment, the independent $log_{10}A$ and B estimates, the predicted free energy barrier $\beta\Delta G = B/[(1-\delta_T)\delta_T^2]$ at $235.5K$, and the predicted nucleation rate (from $J = A\exp[-B/((1-\delta_T)\delta_T^2)]$ at $235.5K$. The separate A and B estimates vary considerably, but they are highly correlated to each other. Fig. 3b shows B vs. $log_{10}A$ for each of the independent estimates. When B is small (large), A is also small (large). The estimated parameters compensate for errors in each other such that all six data sets yield models that predict consistent nucleation rates. The predicted nucleation rates are shown in Table 1 for the temperature $235.5K$.

The measurements of Atkinson et al., were all made in the same way, so the same fundamental nucleation rate expression should describe all six size selected data sets. Accordingly, we reanalyzed the data of Atkinson et al., with one global rate expression ($J = A\exp[-B/((1-\delta_T)\delta_T^2)]$), keeping the same A and B values across all six data sets. The nucleation rate parameters obtained from the global fit are $A = 2.79 \times 10^{46}(cm^{-3}s^{-1})$ and $B = 1.45$. Fig. 3a shows the experimental data for different droplet sizes along with model predictions from the global fit. We emphasize that these are six curves, accurately fitted with just two free parameters, and that both parameters have a clear physical and theoretical interpretation. However, we

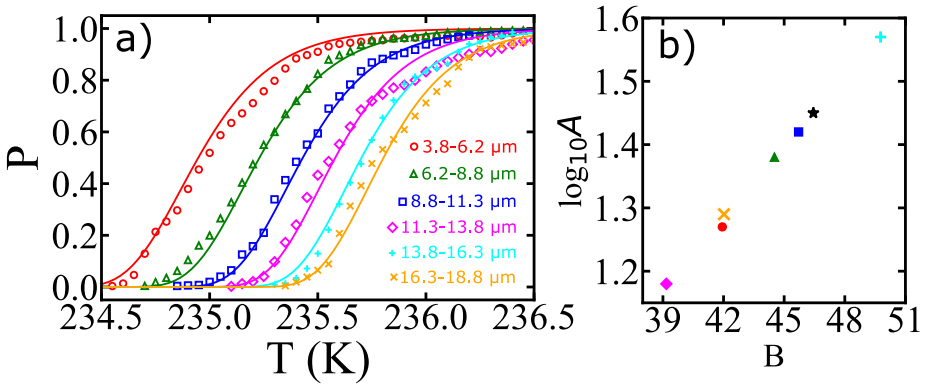

Figure 3. a) Illustration of survival probability fits for homogeneous nucleation with varied droplet sizes at a cooling rate of 1 $K\text{min}^{-1}$. Open symbols represent experimental data from Atkinson et al. (2016) and continuous lines represent model predictions. Colors of symbols indicate different droplet diameters. b) Illustration of the correlation between the $\log_{10} A$ and B parameters obtained from individual fits. Black star indicate the ones obtained by the global fit, and other symbols correspond to estimations for different sizes of droplets.

Droplet size $(D/\mu m)$	$\log_{10} A$	B	$\beta\Delta G_{235.5K}$	$\log_{10} J_{235.5K}$
5.0	41.9	1.27	77.5	8.3
7.5	44.5	1.38	84.2	7.9
10.1	45.7	1.42	86.7	8.1
12.6	39.2	1.18	72.0	7.9
15.1	49.8	1.57	95.8	8.1
17.6	42.0	1.29	78.8	7.8
global	46.4	1.45	88.5	8.0

Table 1. Computed nucleation rate parameters A and B for various groups of droplet sizes using the volume corresponding to the mean diameter of the group. D is the mean diameter of the droplets in the group in μm. $\beta\Delta G$ is the free energy barrier for nucleation, and J is nucleation rate computed using fit parameters in Eq. (6). Estimations of $\beta\Delta G$ and J are corresponding to a temperature of 235.5 K.

note that the theoretical relationship between B and $\beta\Delta G$ reflects only the reversible work to create a nucleus at equilibrium, but the parameter B as obtained from experimental data also reflects activation energy contributions from the prefactor. See Section 9.2 for more explanation about this point.

At a temperature of 235.5 K, the global fit yields a prediction $J = 10^8 cm^{-3} s^{-1}$ for the nucleation rate, consistent with predictions from the independent fits. The free energy barrier at $235.5K$ from the global fit is 88.5 $k_B T$. This is again similar to those obtained from fits to the individual size-selected data sets (Table 1).

Although the rate predictions show remarkable internal consistency, the inferred barriers are scattered and larger than barriers which have been inferred from other data sets (Murray et al. (2010); Shardt et al. (2022); Riechers et al. (2013)). Section 5, explores the effects of size dispersity on inferred rate parameters. Section 6, examines whether size dispersity within the narrow,

but non-zero size-ranges of Atkinson et al., may still affect the inferred rate parameters. The discrepancy may be a consequence of theoretically unaccounted for temperature dependences within the pre-factor. Note that the data sets in cyan and pink Fig. 3a actually cross over each other. The crossover indicates that small droplets are nucleating at warmer temperatures than the larger droplets, which should not occur according to nucleation theory. These two anomalous curves correspond to the two most extreme estimates of A and B (upper right and lower left in Fig. 3b). Thus scatter in the A and B parameters, seems to be a true reflection of experiment-to-experiment variation.

5 Droplets with distribution of volume

Experiments that report on droplet size dispersity (Murray et al. (2010); Shardt et al. (2022); Ando et al. (2018)) consistently report a broader range of sizes than the droplets of Atkinson et al. (2016). This section develops a superposition formula, starting from Eq. (7), for drops of specific sizes, to predict the survival probability for experiments with a broad distribution of droplet sizes. As seen from Fig. 3, large droplets in a broad distribution will nucleate early (at milder supercoolings), while small droplets will survive to deeper supercoolings. The steep sigmoidal survival probabilities for droplets of a specific size, when superimposed, result in a more gradual sigmoid. The gradual sigmoid looks deceptively like the theoretical prediction in Eq. (7), but with artificially reduced barrier B and prefactor A parameters. The analysis here shows how size-dispersity broadens the nucleation spectrum and how the results can potentially affect the inferred nucleation rate parameters.

The joint survival probability distribution with volume and temperature variables is given by

$$P(V,\delta_T) = \rho(V) \times P(\delta_T|V), \tag{9}$$

where $\rho(V)$ is the normalized distribution of droplet volumes and $P(\delta_T|V)$ is the survival probability for droplets of a specific volume, i.e. Eq. (7). The survival probability in time/temperature is obtained by integrating over droplet volumes in the joint distribution.

$$P(\delta_T) = \int_0^\infty P(V,\delta_T)dV. \tag{10}$$

Here we provide an example calculation to illustrate the effects of a broad droplet volume distribution. Let the normalized (gamma-type) distribution of droplet sizes be $\rho(V) = 8V_0^{-2}V\exp(-2V/V_0)$. Here V_0 is the mean volume of the entire range of droplets. Let the survival probability for droplets of any specific size be given by $P(\delta_T|V)$ in Eq. (7), with the global fit values of A and B, as reported in Table 1. The survival probability for the distribution of droplet volumes can then be obtained using Equations 9 and 10.

We let $V_0 = 1057.1\mu m^3$ in $\rho(V)$ to obtain a distribution with droplets of size (diameter) between 3.0 μm and 20 μm. Note that the model volume distribution spans the range of sizes in the experiments of Atkinson et al. Fig. 4, shows the gradually decreasing survival probability from the superposition as a black solid curve with more steeply changing size-selected $P(\delta_T|V)$ data in the background.

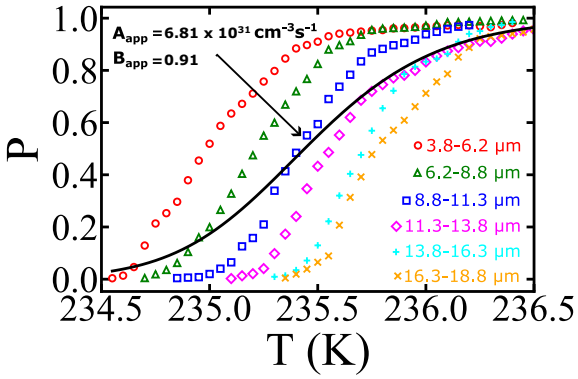

Figure 4. Illustrating the effects of droplet size dispersity on survival probabilities. Open symbols are the experimental survival probabilities for different groups of size-selected droplets from Ref. Atkinson et al. (2016). The continuous black line is the superposition survival probability of Eq. (10) from the same kinetics and for a distribution droplets from 3.8-18.8 μm.

If we were unaware of the droplet polydispersity or did not account for it, we might interpret the black curve in Fig. 4, using a survival probability analysis with nucleation theory for droplets of the mean size V_0. To illustrate how droplet size dispersity influences the inferred nucleation rate parameters, we reoptimized A and B now to minimize the residuals between the dispersity superposition result in $P(\delta_T)$ and the naive specific-volume model $P(\delta_T|V_0)$. The resulting A and B values are $6.81 \times 10^{31} cm^{-3} s^{-1}$ and 0.91 respectively. The inferred prefactor (A_{apparent}) is 15 orders of magnitude smaller than that from the global fit of the sets with narrow volume distribution, and the inferred barrier parameter (B_{apparent}) has been reduced by nearly 40%. Moreover, the inferred free energy barrier at 235.5 K is now estimated to be $\beta\Delta G$ = 55.7 $k_B T$, relative to a value of 88.5 $k_B T$ based on the global fit values to the size selected droplet data. The calculation illustrates how a failure to account for size-dispersity causes a spurious broadening of the nucleation spectrum and reduction in the inferred prefactor A, barrier parameter B, and free energy barriers.

Once we know the variation in droplet sizes, resultant survival probabilities can easily be computed with the help of the python code presented in Section 9 and available in GitHub (https://github.com/Molinero-Group/volume-dispersion). The inputs needed for the program are the proposed distribution of droplet sizes (Gaussian, uniform, gamma, etc.) and the variation of nucleation rate with temperature (see Section 9.1). The output from the code is the effective survival probability.

6 How narrow should a droplet distribution be to safely assume a single volume?

First, we ask whether the range of droplet sizes in each experiment by Atkinson et al., each spanning a few μm, is already broad enough to adversely impact the inferred nucleation parameters. We have considered two test cases for the analysis. One with a midpoint of each reported size range as the size of all droplets in that size range (as shown in the vertical axis of Fig. 5), and the second with a uniform distribution of droplet sizes over the corresponding size ranges (as shown in the horizontal axis of Fig. 5). If the size ranges are sufficiently narrow, these two calculations should result in identical A and B parameters. The

parity plots for the two values of A and B are presented in Fig. 5. As all the data points are close to the x=y line, we conclude that the droplet size ranges in Atkinson et al., are sufficiently narrow to ignore size dispersion when inferring the nucleation kinetics.

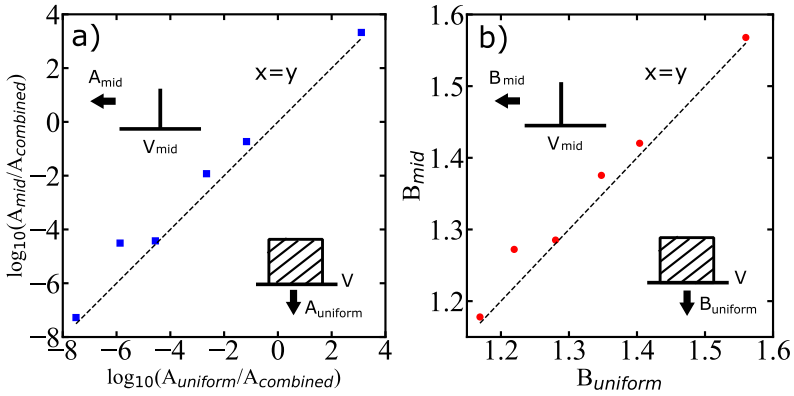

Figure 5. Parity plots showing how droplet size dispersion influences the inferred A and B parameters. Symbols are inferred A and B parameters with a sharp monodisperse droplet distribution (delta function) corresponding to mean size of droplets (mid) as shown in the cartoon on the vertical axis and with a uniform distribution of droplets (uniform) as shown in the cartoon on the horizontal axis. A_{combined} is the prefactor estimated using global fit. Intervals and midpoints in V correspond to size-window of Atkinson et al.. The black dashed lines represent $x = y$ lines (parity).

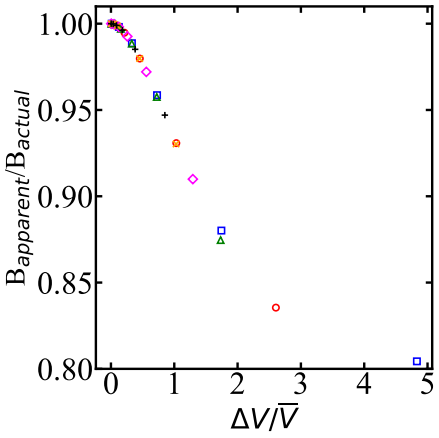

Figure 6. When droplet size dispersity is ignored, the inferred B_{apparent} relative to B_{actual} depends on uniform spread in volume ΔV relative to the mean volume $\bar{V}$. ΔV is the width of a uniform distribution of droplet sizes according to the uniform distribution. Symbols of the same color correspond to different widths of uniform distribution and different colors correspond to different mean size of the droplets. B_{actual} is the predicted B with monodisperse droplets and B_{apparent} is the computed B with dispersity in droplet sizes

Fig. 6 shows the ratio between the apparent B parameter from superposition of survival probabilities of droplets with sizes $\overline{V} \pm \Delta V$ and the true B parameter. The analysis shows that the groups with $2\mu m$ variation in diameter resulted in the same

nucleation rate parameters with approximately less than 1% variation in estimated free energy barriers. Our analysis in Fig. 6 quantifies the effect of dispersion of droplets in the experiments on predicted B parameters, assuming droplets have uniform distribution. Given $\Delta V/\overline{V}$ and B values from an analysis that imposes volume dispersity, Fig. 6 can be used to estimate the true value of B. The analysis shows that to obtain B within 1% of the correct value, the volume dispersity should be no more than 30% of the mean volume.

7 Comparing homogeneous nucleation rate parametrizations

Fig. 7 shows the comparison for the homogeneous nucleation rates using experimental data from Riechers et al. (2013) (blue diamonds) and Atkinson et al. (2016) (green squares). Continuous lines indicate different parametrizations: the fit using the AINTBAD code $J_{hom}^{model}(T)$, where $A = 2.79 \times 10^{46} cm^{-3} s^{-1}$ and $B = 1.45$ for the temperature range of 234.8 to 236.8 K, and $A = 5.72 \times 10^{28} cm^{-3} s^{-1}$ and $B = 0.81$ for 237.0 to 239.1 K (red continuous lines), the parametrization proposed by fitting multiple experimental data $J_{hom}^{equation}(T) = exp[-3.9126T + 939.916]$ Atkinson et al. (2016) (cyan line), as well as the parametrizations based on classical nucleation theory (CNT) from Qiu et al. (2019) (black line) and from Koop and Murray (2016) (magenta line). In a small temperature range, $J_{hom}^{model}(T)$ captures well the experimental data points. The proposed model, $J_{hom}^{model}(T)$, which works well for micrometer-sized droplets at lower temperatures, may have limitations in accurately capturing the complex nucleation processes occurring in larger droplets at higher temperatures. Thus, $J_{hom}^{model}(T)$ can be used only to predict the homogeneous nucleation rate in the temperature range of the input data used to fit the model.

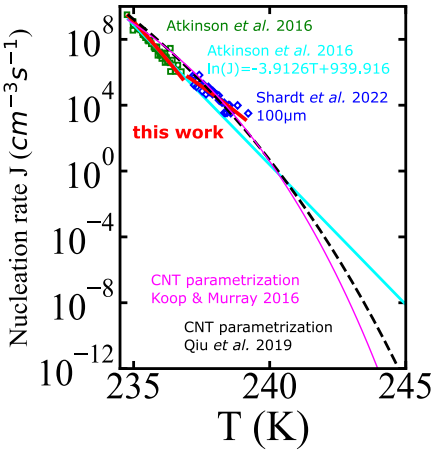

Figure 7. Comparison of the nucleation rate vs. temperature from experiments of Riechers et al. (2013) (blue diamonds) and Atkinson et al. (2016) (green squares); empirical model proposed by Atkinson et al. (2016) (cyan continuous line); global fit A and B in model $J = Aexp[-B/((1-\delta_T)\delta_T^2)]$ fitted to Atkinson et al. (2016) and Shardt et al. (2022) (red continuous lines); and the CNT parametrizations from Qiu et al. (2019) (black dashed line) and Koop and Murray (2016) (magenta continuous line). The temperature axis extends to 245 K, the upper plausible limit of homogeneous nucleation temperatures as defined in Herbert et al. (2015).

All parameterizations predict nucleation rates within an order-of-magnitude of each other and with experiments for temperatures between 235 K and 240 K. However, there is a small gap in the data near 237 K. Fig. 7 suggests a slight disagreement between experimental rates at temperatures below 237 K and those above 237 K. Models for ice nucleation in cloud droplets require nucleation rates that remain accurate over a broad range of temperatures and droplet sizes. Although it is not possible to discriminate between models based on the currently available data, physics-based models should help to build parameterizations that are internally consistent and valid over a broad temperature range.

8 Effect of cooling rate on nucleation parameters

The combined survival probability and nucleation theory expression, as shown in Eq. (7), also predicts that the cooling rate will impact the nucleation spectrum. In this section, we analyze data from Shardt et al. (2022), whose experiments are performed at two different cooling rates (0.1 $K\text{min}^{-1}$ and 1.0 $K\text{min}^{-1}$) with size selected droplets of 75 μm and 100 μm. Shardt et al. report the uncertainty in the droplet sizes to be 5 μm. We model their droplet size distribution using a Gaussian with a mean of 75 (or 100) μm and a standard deviation of 5 μm. We have analyzed the survival probability data across the two droplet sizes and two cooling rates with one global fit. The global fit to the survival probability data across the cooling rates and droplet sizes are shown in Fig. 8. The computed nucleation rate parameters from the global fit are $A = 5.72 \times 10^{28} cm^{-3} s^{-1}$ and $B = 0.81$. The predictions of free energy barriers across the cooling rates and droplet sizes are presented in Table 2.

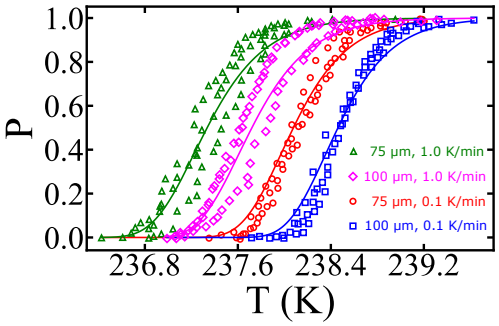

Figure 8. Survival probability fits for homogeneous nucleation data with different droplet sizes and cooling rates. Open circles represent experimental data from Shardt et al. (2022) and the solid lines represent model predictions.

The predictions of B have a similar order of magnitude but are approximately 25% lower when compared to other estimates (Riechers et al. (2013)). We suspect the variation may stem from the difficulties in measuring the precise temperatures of the droplets (Shardt et al. (2022); Tarn et al. (2020); Atkinson et al. (2016)). We also note the computed nucleation rate parameters A and B from Shardt et al., are lower than those from the study of Atkinson et al.. We suspect the reason for this variation might be due to the uncertainty in measurements of temperature of the droplets. The experiments by Shardt et al. indicated the uncertainty in temperature measurements to be $\pm 0.2K$, whereas experiments by Atkinson et al. reports $\pm 0.04K$. The predicted

Size (μm)	R ($K \text{min}^{-1}$)	$\beta \Delta G$	T_{50}/K
75	0.1	57.3	238.4
75	1.0	55.3	237.7
100	0.1	56.4	238.1
100	1.0	54.1	237.3

Table 2. The computed free energy barriers for various droplet sizes across the cooling rates. T_{50} is the temperature corresponding to survival probability of 0.5.

free energy barrier from Atkinson et al. data is 88.5 $k_B T$ at 235.5 K, whereas the free energy barrier from Shardt et al. is 55.3 $k_B T$ at 237.7 K. These predictions contradict nucleation theory which says ΔG decreases as the temperature decreases.

9 A computer code to predict the survival probability using any droplet size distribution and cooling rate

We developed a versatile code capable of taking various parametrizations for the homogeneous nucleation rate $J_{hom}(T)$, the droplet size distributions (Gaussian, Gamma, uniform, exponential, etc.), and cooling rates to compute the survival probability or fraction of frozen droplets. The code IPA (Inhomogeneous Poisson Analysis) is illustrated in Fig. 9. We use the nucleation rate data vs temperature as the input to compute the survival probability using the following equation

$$P(\delta_T|V) = \exp\left[-\left(\frac{VT_m}{R}\right)\int_0^{\delta_T} J(\delta_T')d\delta_T'\right]. \tag{11}$$

Eq. (11) is general representation for any given J and is exactly similar to Eq. (7). We evaluate the integral numerically using the trapezoidal rule. Even though Eq. (11) is strictly valid only for a given constant volume of the droplets, we can use Eq. (11) in combination with Eq. (10) to account for the distribution of sizes. Our code includes diverse nucleation rate variations with temperature, including the local parametrization $J_{hom}^{model}(T)$ discussed in the preceding section, the CNT parametrization from sources like Qiu et al. (2019) and Koop and Murray (2016), and the empirical parametrization from Atkinson et al. (2016). Additionally, users can integrate any other parametrization into the code. The code is publicly accessible at (https://github.com/Molinero-Group/volume-dispersion), last access: 18 Mar 2024).

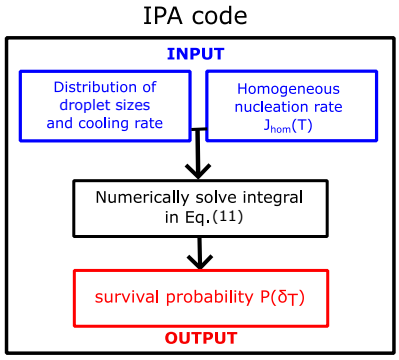

Figure 9. Flowchart of the IPA (Inhomogeneous Poisson Analysis) code to obtain the survival probability of water droplets as a function of temperature for any distribution of droplet sizes, cooling rate, and homogeneous nucleation rate parametrization.

9.1 Survival probability predictions for cloud data using CNT parametrization

To extend $J_{hom}(T)$ to higher temperatures, and predict freezing for any size distribution, we use $J_{hom}^{CNT}(T)$ based on classical nucleation theory (CNT) parametrization of experimental properties of water as previously described in Qiu et al. (2017, 2019). According to CNT, the rate of nucleation is given by

$$J(T) = A(T) \exp\left[\frac{-\Delta G_{hom}}{k_B T}\right], \tag{12}$$

where T is the absolute temperature, k_B is the Boltzmann constant, $A(T)$ is the prefactor, and ΔG_{hom} is the free energy barrier associated with the formation of a critical ice nucleus. The temperature dependence of the prefactor follows the one of the diffusion coefficient of liquid water using the Vogel–Fulcher–Tammann (VFT) model and was obtained from Koop and Murray (2016). The free energy barrier is formulated as

$$\Delta G_{hom} = \frac{16\pi\gamma_{ice-liq}^3}{3\rho^2\Delta\mu^2}, \tag{13}$$

where $\Delta\mu(T)$ is the excess chemical potential of the liquid with respect to the crystal, ρ is the density of the crystal, and $\gamma_{ice-liq}$ is the surface tension of the ice-liquid interface. We follow the procedure developed by Qiu et al. (2019) to compute the homogeneous nucleation rate $J_{hom}(T)$ as a function of experimental properties of water and ice. In summary, the temperature dependence of the free energy barriers is computed with Eq. (13). The ice-liquid surface tension at the melting point was selected to match the $\gamma_{ice-liq}(T_m) = 31.20\ mJm^{-2}$ to match J_{hom} at $T_{hom} = 238K$ for μL droplets cooled at 1 K/min following the experimental data of Atkinson et al. (2016) and Riechers et al. (2013). We approximate the temperature dependence of the ice-liquid surface tension $\gamma_{ice-liq}(T)$ by Turnbull's relation,Turnbull (2004) where $\gamma_{ice-liq}(T)/\gamma_{ice-liq}(T_m) = \Delta H_m(T)/\Delta H_m(T_m)$. This parametrization was previously used in Qiu et al. (2019) to study heterogeneous ice nucleation.

Utilizing the CNT parametrization from Qiu et al. (2019) as an input, we integrate it with diverse droplet size distributions and cooling rates. This integration allows us to explore into the distribution of droplet sizes, varying shape parameters, and their

subsequent freezing behavior. The distribution of water droplets in clouds has been examined through the gamma distribution function Liu et al. (1995); Painemal and Zuidema (2011); Igel and van den Heever (2017). In Fig. 10a, we showcase how different gamma size distributions, manipulated by altering the shape parameter as suggested in Igel and van den Heever (2017), impact droplet sizes. Additionally, Fig. 10b illustrates the survival probability computed via the IPA code under a fixed cooling rate (q_c=1 K/min), demonstrating the influence of varying shape parameters on freezing behavior. Notably, the inset reveals a correlation between the shape parameter and freezing temperature. Furthermore, Fig. 10c examines the effect of cooling rate variation on freezing temperatures. Accurate determination of cloud microphysical properties, as explored through these analyses, is crucial for improving climate modeling accuracy.

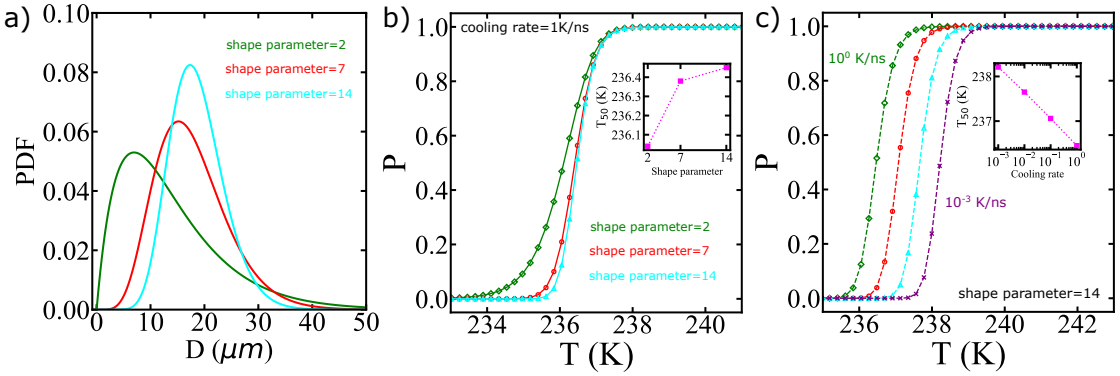

Figure 10. We use the CNT parametrization from Qiu et al. (2019) as an input, and we integrate it with diverse droplet size distributions and cooling rates. a) We employ a gamma distribution characterized by different shape parameters as used in Igel and van den Heever. b) The survival probability predictions for the distributions shown in a) and cooling rates $q_c = 1$ K/min. c) The survival probability predictions using the same droplet size distribution but with varying cooling rate.

9.2 B as obtained from experiment reflects both diffusion and nucleation barriers

To demonstrate another aspect of the IPA code, we applied a Gaussian distribution with a mean droplet diameter of 5μm and a spread of 0.5μm, as shown in Fig. 11a. Using a cooling rate of 1 K min^{-1} and the $J_{hom}^{CNT}(T)$ parametrization from Qiu et al. (2019), we utilized the IPA code to predict the survival probability (blue circles in Fig. 11b). Subsequently, our AINTBAD code was employed to extract parameters A, B, ΔG, and T_{50}. In Table 1, droplet sizes vary from 3.8 to 18.8 μm with corresponding free energy barriers between 72.0 and 95.8 k_BT. Additionally, Table 2 presents sizes of 75 and 100 μm with barriers ranging from 54.1 to 57.3 k_BT. While one might anticipate smaller ΔG for smaller droplets, our observations reveal the opposite trend. Note that the values of ΔG and T_{50} obtained from the code align closely with the sum of free energy barriers for diffusion and homogeneous nucleation, computed using the CNT parametrization from Qiu et al. (2019), as depicted in Fig. 11c. We note that diffusion barriers in supercooled water may also influence inferred values of A, B, and $\beta\Delta G$ as obtained from experiments with the AINTBAD code.

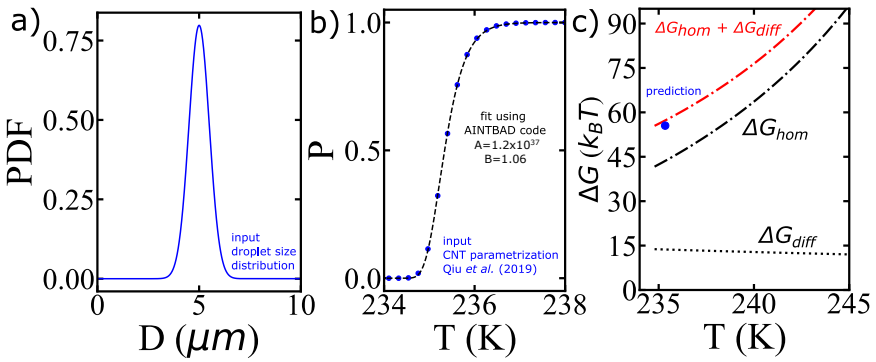

Figure 11. a) Distribution of droplet sizes, b) survival probability prediction using the IPA code and the CNT parametrization from Qiu et al. (2019) (blue circles) and the fit using the AINTBAD code (black dashed line), and c) comparison between the nucleation barriers computed using the CNT parametrization from Qiu et al. (2019) and the predicted one from the model.

10 Impact of temperature uncertainty on the apparent nucleation barriers

Another important factor that has a significant effect on the measured nucleation spectrum is the measurement of droplet temperature. The estimations of the droplet temperatures in freezing experiments show large variability (Tarn et al. (2020); Shardt et al. (2022)). The highest level of accuracy in the temperature measurements is $\pm 0.2K$ (Shardt et al. (2022)).

In this study, we conducted a sensitivity analysis using our model to quantify the impact of temperature measurement uncertainty on estimated free energy barriers. To perform this analysis, we utilized data from frozen 75 μm droplets, as presented in Shardt et al. (2022), which were collected at a cooling rate of 0.1 K/min. Through the HUB-backward code de Almeida Ribeiro et al. (2023), we determined the optimized differential spectra denoted as $n_m(T)$ based on the frozen fraction (represented by the red continuous line in Fig. 12a). The resulting parameters derived from this analysis were $T_{\text{mode}} = 238.2$K and $s = 0.33$, where T_{mode} represents the most probable freezing temperature within the distribution, and s characterizes the distribution's spread. Subsequently, we employed the original distribution (red continuous line in Fig. 12b) to generate random temperature values, augmenting them with random values drawn from a uniform distribution within the range of -0.4 to +0.4 (or -0.2 to 0.2). These additional values introduce noise into the data. We sampled a total of 100 temperature values, equivalent to simulating the behavior of 100 droplets in an experimental setup. The resulting differential freezing spectra is illustrated by the blue squares and green triangles in Fig. 12b. For each case, we calculated the survival probability and fitted the data using Eq. (7), resulting in the continuous lines depicted in Fig. 12c. The effects of temperature variation on the nucleation spectrum are summarized in Table 3. We conclude that measurements with $\pm 0.2K$ and $\pm 0.4K$ variations, resulted in 8% and 14% variation in the computed free energy barriers, respectively. Even though the predictions of free energy barriers show a strong dependence on the uncertainty in temperature measurements, the nucleation rates are insensitive as shown in Table 3. However, the noise in the predicted rate data increases with the noise in temperature measurements.

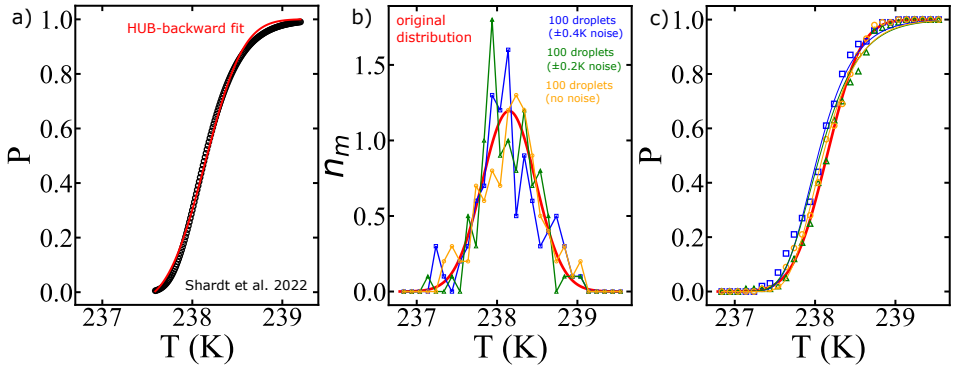

Figure 12. Illustration of the effect of temperature uncertainty on the nucleation spectrum. a) We use the HUB-backward code, (de Almeida Ribeiro et al. (2023)) to find the best fit (continuous red line) of the experimental data Shardt et al. (2022) (black circles). b) The continuous red line shows the optimized differential spectra denoted as $n_m(T)$, with resulting parameters $T_{\text{mode}} = 238.2\text{K}$ and $s = 0.33$, where T_{mode} represents the most probable freezing temperature within the distribution, and s characterizes the distribution's spread. We use the red continuous line as the original distribution to generate 100 temperature values (orange circles). Random noise is introduced in the temperature (± 0.4 K shown in blue squares, ± 0.2 K shown in green triangles). c) The survival probability fit (continuous lines) of the artificially generated data based on Eq. (8).

Noise (K)	B	$\beta\Delta G$	$\log_{10}(J_{238.2K})$
0.0	0.97 $\pm$0.05	67.0 $\pm$3.0	5.06 $\pm$ 0.03
0.2	0.89 $\pm$0.06	62.0 $\pm$4.0	5.01 $\pm$ 0.04
0.4	0.83 $\pm$ 0.03	58.0 $\pm$2.0	5.05 $\pm$ 0.07

Table 3. The computed free energy barriers and nucleation rates for various uncertainties in the temperature measurements. Mean and standard deviation of B and $\beta\Delta G$ are computed from 5 different estimates. We consider T_{50} to be 238.2K for all the cases presented in this table.

11 Conclusions

Homogeneous nucleation can be studied in experiments that record the freezing temperature as ultrapure nanoscale water droplets are gradually cooled to temperatures far below 0^0C. Some prior studies have analyzed these experiments using Poisson statistics and survival probabilities. Others have analyzed with numerical theories. We combined a stochastic survival probability analysis with classical nucleation theory (CNT). The combined framework allows us to account for both droplet size distribution and cooling rate while extracting prefactor and barrier parameters in CNT type rate expression. We applied it to analyze the homogeneous nucleation data obtained from two different studies: Atkinson et al. (2016); Shardt et al. (2022). We first used the new framework to extract parameters and rate expressions from experiments on six groups of size selected droplets, from $5.0 \pm 1.2\mu m$ to $17.5 \pm 1.2\mu m$. The analysis gave similar prefactors, barriers and rates across all six experiments. We further showed that all six experiments can be fitted with just two parameters from one global parameterization. We derived

a superposition formula to show that a distribution of droplet volumes causes a broadening of the distribution of nucleation temperatures. We demonstrate that ignoring volume dispersity in analysis of nucleation temperatures causes an artificial reduction in the inferred barrier and prefactor values. Finally, we applied our model to analyze data from experiments with variations in cooling rates and droplet sizes Shardt et al. (2022).

We present two Python codes AINTBAD and IPA. AINTBAD uses the nucleation spectrum from drop-freezing experiments to estimate theoretically motivated rate parameters from nucleation theory. AINTBAD directly optimizes the rate parameters from the cumulative frozen fraction vs. temperature data. It does not require large number of droplets to estimate nucleation rates at each temperature like other procedures. Although the AINTBAD code does not directly use nucleation rates in the optimization, it does yield highly accurate and robust estimates of the nucleation rate. The IPA code can predict the nucleation spectrum for any given distribution of droplet sizes, any cooling rate, and for any nucleation rate expression. We have demonstrated its application for rates estimated from experiments and for rates predicted using theoretical models. Even though we restrict our discussion to homogeneous nucleation data in this article, it should be possible to develop similar methods for heterogeneous nucleation data. A key challenge is that volume dispersity multiplies only the homogeneous nucleation prefactor in a collection of pure water droplets, while the surfaces that promote heterogeneous nucleants will vary both in area (prefactor) and contact angle (barrier).

Code availability. The codes and data that support the findings of this study are available in the github repository https://github.com/Molinero-Group/volume-dispersion

Author contributions. RKRA, IdAR, VM and BP designed the project and prepared the manuscript. RKRA, IdAR and BP developed the model and performed the analysis.

Competing interests. The contact author has declared that none of the authors has any competing interests

Acknowledgements. We thank Geoffrey Poon, Max Flattery and Conrad Morris for helpful discussions. This work was supported by the Air Force Office of Scientific Research through MURI Award FA9550-20-1-0351.

References

Alpert, P. A. and Knopf, D. A.: Analysis of isothermal and cooling-rate-dependent immersion freezing by a unifying stochastic ice nucleation model, Atmos. Chem. Phys., 16, 2083–2107, 2016.

Ando, K., Arakawa, M., and Terasaki, A.: Freezing of micrometer-sized liquid droplets of pure water evaporatively cooled in a vacuum, Phys. Chem. Chem. Phys., 20, 28 435–28 444, 2018.

Atkinson, J. D., Murray, B. J., and O'Sullivan, D.: Rate of Homogenous Nucleation of Ice in Supercooled Water, J. Phys. Chem. A, 120, 6513–6520, 2016.

Barrett, A. I., Westbrook, C. D., Nicol, J. C., and Stein, T. H. M.: Rapid ice aggregation process revealed through triple-wavelength Doppler spectrum radar analysis, Atmos. Chem. Phys., 19, 5753–5769, 2019.

Becker, R. and Döring, W.: Kinetische Behandlung der Keimbildung in übersättigten Dämpfen, Annalen der Physik, 416, 719–752, 1935.

Cox, D. and Oakes, D.: Analysis of Survival Data, Chapman & Hall/CRC Monographs on Statistics & Applied Probability, Taylor & Francis, https://books.google.com/books?id=Y4pdM2soP4IC, 1984.

de Almeida Ribeiro, I., Meister, K., and Molinero, V.: HUB: a method to model and extract the distribution of ice nucleation temperatures from drop-freezing experiments, Atmospheric Chemistry and Physics, 23, 5623–5639, 2023.

Deck, L. T., Ochsenbein, D. R., and Mazzotti, M.: Stochastic shelf-scale modeling framework for the freezing stage in freeze-drying processes, Int. J. Pharm., 613, 121 276, 2022.

DeMott, P. J., Prenni, A. J., Liu, X., Kreidenweis, S. M., Petters, M. D., Twohy, C. H., Richardson, M. S., Eidhammer, T., and Rogers, D. C.: Predicting global atmospheric ice nuclei distributions and their impacts on climate, Proc. Natl. Acad. Sci. U.S.A., 107, 11 217–11 222, 2010.

Deville, S.: Ice-Templating: Processing Routes, Architectures, and Microstructures, pp. 171–252, Springer International Publishing, Cham, 2017.

Dobbie, S. and Jonas, P.: Radiative influences on the structure and lifetime of cirrus clouds, Q. J. R. Meteorol. Soc., 127, 2663–2682, 2001.

Goff, H.: Colloidal aspects of ice cream—A review, Int. Dairy J., 7, 363–373, 1997.

Herbert, R. J., Murray, B. J., Whale, T. F., Dobbie, S. J., and Atkinson, J. D.: Representing time-dependent freezing behaviour in immersion mode ice nucleation, Atmos. Chem. Phys., 14, 8501–8520, 2014.

Herbert, R. J., Murray, B. J., Dobbie, S. J., and Koop, T.: Sensitivity of liquid clouds to homogenous freezing parameterizations, Geophysical Research Letters, 42, 1599–1605, 2015.

Ickes, L., Welti, A., and Lohmann, U.: Classical nucleation theory of immersion freezing: sensitivity of contact angle schemes to thermodynamic and kinetic parameters, Atmos. Chem. Phys., 17, 1713–1739, 2017.

Igel, A. L. and van den Heever, S. C.: The importance of the shape of cloud droplet size distributions in shallow cumulus clouds. Part II: Bulk microphysics simulations, Journal of the Atmospheric Sciences, 74, 259–273, 2017.

John Morris, G., Acton, E., Murray, B. J., and Fonseca, F.: Freezing injury: The special case of the sperm cell, Cryobiology, 64, 71–80, 2012.

Kashchiev, D.: Nucleation : basic theory with applications, 2000.

Knopf, D. A. and Alpert, P. A.: Atmospheric ice nucleation, Nat. Rev. Phys., 5, 203–217, 2023.

Knopf, D. A., Alpert, P. A., Zipori, A., Reicher, N., and Rudich, Y.: Stochastic nucleation processes and substrate abundance explain time-dependent freezing in supercooled droplets, NPJ Clim. Atmos. Sci., 3, 2, 2020.

Koop, T. and Murray, B. J.: A physically constrained classical description of the homogeneous nucleation of ice in water, The Journal of Chemical Physics, 145, 211 915, 2016.

Koop, T., Luo, B., Tsias, A., and Peter, T.: Water activity as the determinant for homogeneous ice nucleation in aqueous solutions, Nature, 406, 611–614, 2000.

Kubota, N.: Random distribution active site model for ice nucleation in water droplets, CrystEngComm, 21, 3810–3821, 2019.

Laksmono, H., McQueen, T. A., Sellberg, J. A., Loh, N. D., Huang, C., Schlesinger, D., Sierra, R. G., Hampton, C. Y., Nordlund, D., Beye, M., Martin, A. V., Barty, A., Seibert, M. M., Messerschmidt, M., Williams, G. J., Boutet, S., Amann-Winkel, K., Loerting, T., Pettersson, L. G. M., Bogan, M. J., and Nilsson, A.: Anomalous Behavior of the Homogeneous Ice Nucleation Rate in "No-Man's Land", J. Phys. Chem. Lett., 6, 2826–2832, 2015.

Laval, P., Crombez, A., and Salmon, J. B.: Microfluidic Droplet Method for Nucleation Kinetics Measurements, Langmuir, 25, 1836–1841, 2009.

Li, B. and Sun, D.: Novel methods for rapid freezing and thawing of foods – a review, J. Food Eng., 54, 175–182, 2002.

Liu, Y., Laiguang, Y., Weinong, Y., and Feng, L.: On the size distribution of cloud droplets, Atmospheric Research, 35, 201–216, https://doi.org/https://doi.org/10.1016/0169-8095(94)00019-A, 1995.

Marcolli, C., Gedamke, S., Peter, T., and Zobrist, B.: Efficiency of immersion mode ice nucleation on surrogates of mineral dust, Atmos. Chem. Phys., 7, 5081–5091, 2007.

Möhler, O., DeMott, P. J., Vali, G., and Levin, Z.: Microbiology and atmospheric processes: the role of biological particles in cloud physics, Biogeosciences, 4, 1059–1071, 2007.

Murray, B. J., Broadley, S. L., Wilson, T. W., Bull, S. J., Wills, R. H., Christenson, H. K., and Murray, E. J.: Kinetics of the homogeneous freezing of water, Phys. Chem. Chem. Phys., 12, 10 380–10 387, 2010.

Painemal, D. and Zuidema, P.: Assessment of MODIS cloud effective radius and optical thickness retrievals over the Southeast Pacific with VOCALS-REx in situ measurements, Journal of Geophysical Research: Atmospheres, 116, 2011.

Qiu, Y., Odendahl, N., Hudait, A., Mason, R. H., Bertram, A. K., Paesani, F., DeMott, P. J., and Molinero, V.: Ice Nucleation Efficiency of Hydroxylated Organic Surfaces Is Controlled by Their Structural Fluctuations and Mismatch to Ice., Journal of the American Chemical Society, 139 8, 3052–3064, 2017.

Qiu, Y., Hudait, A., and Molinero, V.: How Size and Aggregation of Ice-Binding Proteins Control Their Ice Nucleation Efficiency, Journal of the American Chemical Society, 141, 7439–7452, 2019.

Riechers, B., Wittbracht, F., Hütten, A., and Koop, T.: The homogeneous ice nucleation rate of water droplets produced in a microfluidic device and the role of temperature uncertainty, Phys. Chem. Chem. Phys., 15, 5873–5887, 2013.

Sear, R. P.: Nucleation: theory and applications to protein solutions and colloidal suspensions, J. Phys. Condens. Matter., 19, 033 101, 2007.

Sear, R. P.: Quantitative studies of crystal nucleation at constant supersaturation: experimental data and models, CrystEngComm, 16, 6506–6522, 2014.

Shardt, N., Isenrich, F. N., Waser, B., Marcolli, C., Kanji, Z. A., deMello, A. J., and Lohmann, U.: Homogeneous freezing of water droplets for different volumes and cooling rates, Phys. Chem. Chem. Phys., 24, 28 213–28 221, 2022.

Shultz, M. J.: Crystal growth in ice and snow, Phys. Today., 71, 34–39, 2018.

Sibley, D. N., Llombart, P., Noya, E. G., Archer, A. J., and MacDowell, L. G.: How ice grows from premelting films and water droplets, Nat. Commun., 12, 239, 2021.

Stan, C. A., Schneider, G. F., Shevkoplyas, S. S., Hashimoto, M., Ibanescu, M., Wiley, B. J., and Whitesides, G. M.: A microfluidic apparatus for the study of ice nucleation in supercooled water drops, Lab Chip, 9, 2293–2305, 2009.

Stoll, N., Eichler, J., Hörhold, M., Shigeyama, W., and Weikusat, I.: A Review of the Microstructural Location of Impurities in Polar Ice and Their Impacts on Deformation, Front. Earth Sci., 8, 2021.

Stöckel, P., Weidinger, I. M., Baumgärtel, H., and Leisner, T.: Rates of Homogeneous Ice Nucleation in Levitated H2O and D2O Droplets, J. Phys. Chem. A, 109, 2540–2546, 2005.

Tarn, M. D., Sikora, S. N. F., Porter, G. C. E., Wyld, B. V., Alayof, M., Reicher, N., Harrison, A. D., Rudich, Y., Shim, J. u., and Murray, B. J.: On-chip analysis of atmospheric ice-nucleating particles in continuous flow, Lab Chip, 20, 2889–2910, 2020.

Turnbull, D.: Formation of Crystal Nuclei in Liquid Metals, Journal of Applied Physics, 21, 1022–1028, 2004.

Volmer, M. and Weber, : Keimbildung in übersättigten Gebilden, Zeitschrift für Physikalische Chemie, 119U, 277–301, https://doi.org/doi:10.1515/zpch-1926-11927, 1926.

Wright, T. P. and Petters, M. D.: The role of time in heterogeneous freezing nucleation, J. Geophys. Res. Atmos., 118, 3731–3743, 2013.

Zachariassen, K. E. and Kristiansen, E.: Ice Nucleation and Antinucleation in Nature, Cryobiology, 41, 257–279, 2000.

Zhang, X. and Maeda, N.: Nucleation curves of ice in the presence of nucleation promoters, Chem. Eng. Sci., 262, 118 017, 2022.